

# Virtual sensor fusion for high precision control

Mohit Verma<sup>a,\*</sup>, Thomas Dehaeze<sup>b</sup>, Guoying Zhao<sup>a</sup>, Jennifer Watchi<sup>a</sup>, Christophe Collette<sup>a,b</sup>

<sup>a</sup>*Université Libre de Bruxelles, Precision Mechatronics Laboratory, BEAMS Department, 50, F.D. Roosevelt av., 1050 Brussels, Belgium.*

<sup>b</sup>*University of Liège, Department of Aerospace and Mechanical Engineering, Allée de la Découverte 9, 4000 Liège, Belgium.*

---

## Abstract

High performance control requires high loop gain and large control bandwidth. However, the spurious resonances at the higher frequencies can limit the performance of such type of systems. This drawback can be overcome by using sensor fusion technique. In sensor fusion, two different sensors are combined in synergy such that good performance is achieved at lower frequencies while ensuring robustness of the system at higher frequencies. This paper presents a new technique, termed as “virtual sensor fusion”, in which only one of the sensors is physically installed on the system while the other sensor is simulated virtually. The other sensor is selected based on desired high frequency response. The effectiveness of the proposed technique is demonstrated numerically for a case of active seismic isolation. A robustness analysis of virtual sensor fusion is also carried out in order to study its stability in the presence of spurious resonances. Finally, the technique is experimentally verified on active isolation of pendulum system from ground motion. The results obtained demonstrate good isolation performance at lower frequencies and robustness to plant uncertainties (spurious resonances) at higher frequencies. This technique can be effectively used for high precision control of sensitive instruments.

*Keywords:*

sensor fusion, precision, vibration isolation, active control, virtual sensor

---

## 1. Introduction

Precision control applications can be broadly classified into two major categories [1] — disturbance rejection and pointing control. Disturbance rejection involves the isolation of an equipment

---

\*Corresponding author

*Email address:* mohit.verma@ulb.ac.be (Mohit Verma)

from a source of vibration or ground motion. Seismic isolation of large physics instruments like LIGO is one such example [2, 3]. Pointing control usually involves tracking or alignment of the reference to a receptor. Tracking the position of a star and telecommunication are some examples where pointing control is required. Also, there are certain applications which require both active isolation and pointing control. For example, microvibration control for high pointing accuracy in space systems [4].

In precision control, the gain of the controller is usually set to a very large value in order to achieve the desired performance. This often destabilize the system due to amplification of the internal modes. This can be avoided by collocating sensor and actuator pair. The collocated system has alternating poles and zeros, which guarantees the stability of the system [5]. However, it is not always possible to collocate sensor and actuator pair due to size and space limitations. Even if they are collocated, there are chances that the high frequency flexible modes of the structure might get excited [6]. This limits the bandwidth and the performance of the precision control system. A possible solution to address this issue consists of adding a notch filter at the location of the internal resonances [3, 7]. Another way is to passively damp the spurious resonance using tuned mass dampers (TMD) [8, 9] or dynamic vibration absorbers (DVA) [10]. A major drawback of these solutions is that they require a good knowledge of the plant and the location of the spurious resonance. Also, the variations in the properties of the plant with time will shift the location of the spurious resonance and thus, will render the solution inefficient.

As precision control has to operate in a limited frequency range, one of the effective ways is to use sensor fusion [11]. In sensor fusion two different sensor are used — one sensor is used to achieve good performance in the region of interest while the other imparts stability to the system beyond the region of interest [12]. Sensor fusion also has the ability to mitigate DC drifts [13]. The use of sensor fusion for active vibration isolation was explored in [14] and this paper further develops those ideas. This paper presents *virtual sensor fusion* in which only one sensor is mounted on the structure while the other sensor is simulated virtually using a digital filter. The control architecture forms an inner loop with the virtual sensor and an outer loop with the real sensor. Various model based control methods also use a similar kind of control architecture. For example, internal model control [15–17] and disturbance observer based control [18–22] use a model of the plant in the inner loop. The difference between the responses of the real plant and the model (due to un-

certainties and/or unmodeled plant dynamics) is then used to drive the controller with the objective of disturbance rejection. The control architecture of virtual sensor fusion is motivated from model based control methods. However, the key difference here is the role of the inner loop. In model based methods, inner loop is added with the aim of achieving good disturbance rejection. However in virtual sensor fusion, the inner loop is added to impart stability to the system in the high frequency region. Also, the inner loop does not necessarily include the model of the plant in virtual sensor fusion. It can be any stable transfer function with the desired high frequency response, provided that it has the same gain and slope as the real plant in the vicinity of the merging frequency, for ensuring a smooth transition between the real plant and the virtual plant. We demonstrate, through numerical and experimental investigations, that virtual sensor fusion provides good isolation performance in low frequency region while ensuring stability of the system to high frequency spurious resonances.

The organization of this paper is as follows. Section 2 describes the general framework for virtual sensor fusion. It demonstrates how the control input is decoupled from the high frequency spurious resonances of the plant. Virtual sensor fusion is then applied to active seismic vibration isolation system in Section 3. This is followed by robust stability analysis of the same system studied in Section 4. Finally, the experiments carried out towards the validation of virtual sensor fusion on a pendulum system are presented in Section 5 followed by concluding remarks in Section 6.

## 2. Control architecture

A generalized framework for virtual sensor fusion is shown in Figure 1. A real sensor (inertial sensor is used in the present study) is used at low frequencies to provide good performance while a virtual sensor is used at high frequencies to ensure stability of the closed loop system. The virtual sensor is the output of a virtual plant,  $G_v$ , designed to dominate the control command at high frequency. It does not need to mimic a physical quantity of the real plant. The sensors are augmented with filters such that the control input is dominated by the real sensor at lower frequencies and by virtual sensor at higher frequencies. A new sensor is constructed by fusing the signals from the inertial and virtual sensors. In Figure 1,  $K$  is the controller to be designed,  $G_u$  is the plant,  $G_v$  is the virtual sensor,  $H_L$  is the low pass filter,  $H_H$  is the high pass filter,  $r$  is the reference signal (equal to zero in case of isolation system),  $u$  is the control input to the plant,  $y$  is the output to

be regulated,  $d$  is the disturbance acting at the output of the plant and  $n$  is the measurement noise. Based on the block diagram, the output to be regulated is equal to

$$y = \frac{1 + KG_v H_H}{1 + L} d + \frac{KG_u}{1 + L} r - \frac{KG_u H_L}{1 + L} n \quad (1)$$

where  $L = K(G_v H_H + G_u H_L)$  is the loop gain. The response of high pass filter  $H_H$  is negligible at low frequency (i.e,  $H_H \approx 0$ ). From the above equation, it is observed that good tracking performance or disturbance rejection can be obtained if a large value of gain is chosen for the controller  $K$  at low frequency. In classical control architecture, a large value of the gain can render the closed loop system unstable in the presence of high frequency spurious resonances. However, such problems are bypassed if we use virtual sensor fusion. This can be demonstrated by observing the control input to the plant. The control input,  $u$ , is given by

$$u = -\frac{KH_L}{1 + L} d + \frac{K}{1 + L} r - \frac{KH_L}{1 + L} n \quad (2)$$

The control input at the lower frequencies can be approximated as

$$u = -\frac{K}{1 + KG_u} d + \frac{K}{1 + KG_u} r - \frac{K}{1 + KG_u} n \quad (3)$$

It can be seen that at low frequency, the control input solely depends on the measurements from the sensor mounted on the actual structure (inertial control). Similarly it can be shown that at higher frequencies, where the transfer function  $H_L \approx 0$ , the control input can be written as

$$u = \frac{K}{1 + KG_v H_H} r \quad (4)$$

The control input at high frequency depends only on the virtual sensor. Thus, the instability that might occur due to the spurious resonances of the system at the higher frequencies is avoided as they do not appear in the feedback loop.

The stability of the closed system can be assessed by investigating the frequency response of the open loop,  $L$ . However, this is not sufficient in case of virtual sensor fusion because of the inner-loop. The control signal  $u$  and  $y$  are related by the following transfer function

$$G_{inner} = \frac{KH_L}{1 + KG_v H_H} \quad (5)$$

The stability of the above transfer function should also be checked in addition to the overall stability of the closed loop system. Actually, in the frequency range below the merging, an additional

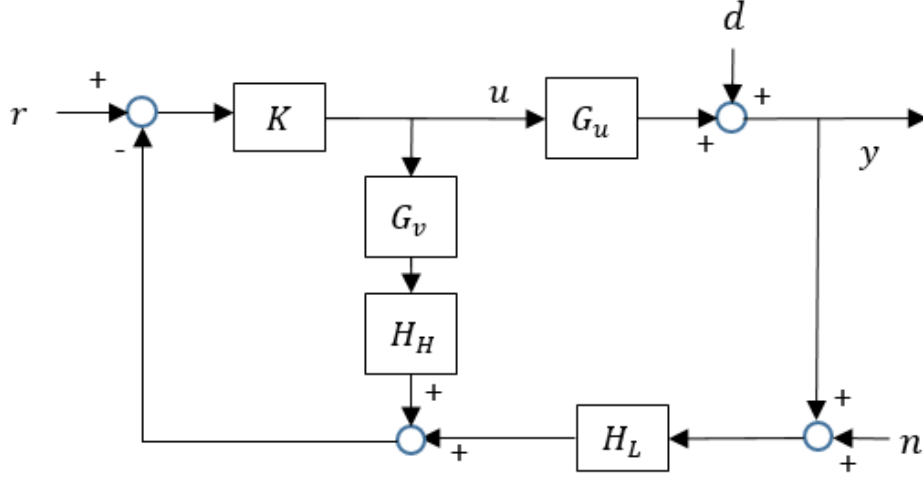


Figure 1: Generalized framework for virtual sensor fusion — A virtual sensor,  $G_v$ , is used in the inner loop. Real sensor dominates at the low frequencies while virtual sensor dominates at the high frequencies. This control strategy avoids the spurious resonances of the plant from appearing in the controller feedback loop.

constraint might be imposed on  $K$  for ensuring the stability of the internal loop, because the two loops do not have the same gain at low frequency. However, if the stability of the full system (equation (1)) is conditional, the stability of the internal loop is automatically guaranteed.

### 3. Active vibration isolation using virtual sensor fusion

In this section, we demonstrate the application of virtual sensor fusion for vibration isolation. The payload to be isolated is constituted of two masses  $m_1$  and  $m_2$ , linked by a stiffness  $k_2$  and a dashpot  $c_2$  in order to represent the flexibility of the payload. It is assumed that the motion of the top mass is measured by an ideal sensor. The input of the controller is the inertial motion of the top mass,  $x_2$  and the output is the control force,  $u$ . The dynamic equations of motion of the system under consideration can be written as

$$m_1 s^2 x_1 + (k_1 + c_1 s)(x_1 - w) + (k_2 + c_2 s)(x_1 - x_2) = u \quad (6)$$

$$m_2 s^2 x_2 + (k_2 + c_2 s)(x_2 - x_1) = 0 \quad (7)$$

where  $s$  is a Laplace transform variable. From equation (6), motion of mass  $m_1$  can be written as

$$x_1 = \frac{u + (k_1 + c_1 s)w + (k_2 + c_2 s)x_2}{m_1 s^2 + (c_1 + c_2)s + (k_1 + k_2)} \quad (8)$$

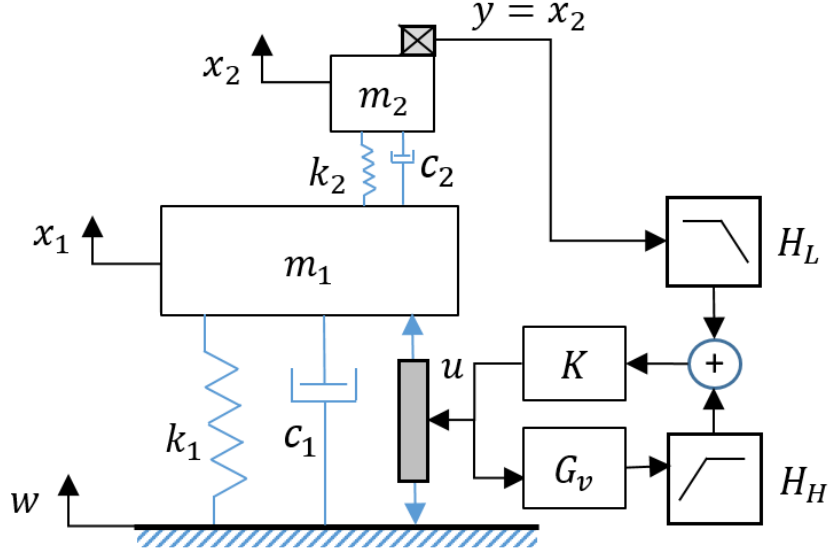


Figure 2: Virtual sensor fusion applied to the active vibration isolation — The bottom spring-mass-dashpot system represents the system to be isolated while the top represents sensor dynamics. Inertial sensor control is used at low frequencies while virtual sensor control is used at high frequencies. This is achieved by passing the inertial and virtual sensor signals through low and high pass filters.

Substituting equation (8) in (7), we get

$$x_2 = G_1 u + G_2 w \quad (9)$$

where

$$G_1 = \frac{k_2 + c_2 s}{(m_1 s^2 + (c_1 + c_2) s + k_1 + k_2)(m_2 s^2 + c_2 s + k_2) - (k_2 + c_2 s)^2}$$

$$G_2 = \frac{(k_1 + c_1 s)(k_2 + c_2 s)}{(m_1 s^2 + (c_1 + c_2) s + k_1 + k_2)(m_2 s^2 + c_2 s + k_2) - (k_2 + c_2 s)^2}$$

Similarly, the motion of mass  $m_1$  can be expressed as

$$x_1 = G_3 u + G_4 w \quad (10)$$

where transfer functions  $G_3$  and  $G_4$  can be obtained by substituting equation (9) in (8).

The transfer function from  $u$  to  $y$  ( $G_u$ ) in Figure 1 is equal to

$$G_u = \frac{k_2 + c_2 s}{(m_1 s^2 + (c_1 + c_2) s + k_1 + k_2)(m_2 s^2 + c_2 s + k_2) - (k_2 + c_2 s)^2} \quad (11)$$

The system to be isolated has a mass of 20 kg. The natural frequency and damping ratio are 2 Hz and 1%, respectively. The mass, natural frequency and damping ratio corresponding to the

sensor dynamics are taken as 0.5 kg, 500 Hz and 1%, respectively. The merging frequency ( $\omega_f$ ) of the filters is set as 50 Hz. The filters are chosen to be complementary to avoid zeros that might creep in due to merging [14]. Fifth order complementary filters are used in the present study whose transfer functions are given by

$$H_L = \frac{1.2865 \times 10^{-16}(s + 3.54 \times 10^7)(s + 26.24)(s + 6.541)(s^2 - 3.54 \times 10^7 s + 1.253 \times 10^{15})}{(s + 622)(s + 62.83)(s + 6.347)(s^2 + 62.83s + 3948)}$$

$$H_H = \frac{s^3(s + 603.5)(s + 150.4)}{(s + 622)(s + 62.83)(s + 6.347)(s^2 + 62.83s + 3948)}$$
(12)

The frequency responses of the filters are shown in Figure 3. A lead-lag compensator is used as a controller,  $K$ . Lag ensures high loop gain at lower frequencies while lead provides sufficient gain margins at higher frequencies. The transfer function of the controller used is

$$K = \frac{1.5791 \times 10^5(s + 23.84)(s + 2)}{(s + 238.4)(s + 0.2)}$$
(13)

The virtual sensor is chosen in such a way that its response near the blending frequency has the same gain and same slope as the real plant. This avoids the undesirable zeros that might appear due to blending. It is assumed that we have a good model of the plant near the blending frequency. One of the simplest choices for virtual sensor ( $G_v$ ) is the model of the system to be isolated. That is,

$$G_v = \frac{1}{m_1 s^2 + c_1 s + k_1}$$
(14)

The comparison of the frequency response of the plant before fusion,  $G_u$ , and the plant after fusion ( $G_v H_H + G_u H_L$ ) is shown Figure 4. It can be seen that there is no phase degradation due to sensor dynamics in the plant after fusion. The comparison of the transfer functions from inertial control, virtual sensor control and their fusion to  $x_2$  is shown in Figure 5. It reassures the fact that inertial control is dominant at low frequency while virtual sensor control becomes dominant at high frequency in virtual sensor fusion. The transmissibilities (i.e., the magnitude of the transfer function from  $w$  to  $x_1$ ) of the open and closed loop systems are compared in Figure 6. The virtual sensor fusion provides good isolation performance below 10 Hz.

#### 4. Robustness to real plant uncertainty

In this section we demonstrate the robust stability of virtual sensor fusion for the same system studied in the previous section. To this purpose, we will represent the real plant ( $G_u$ ) as a perturba-

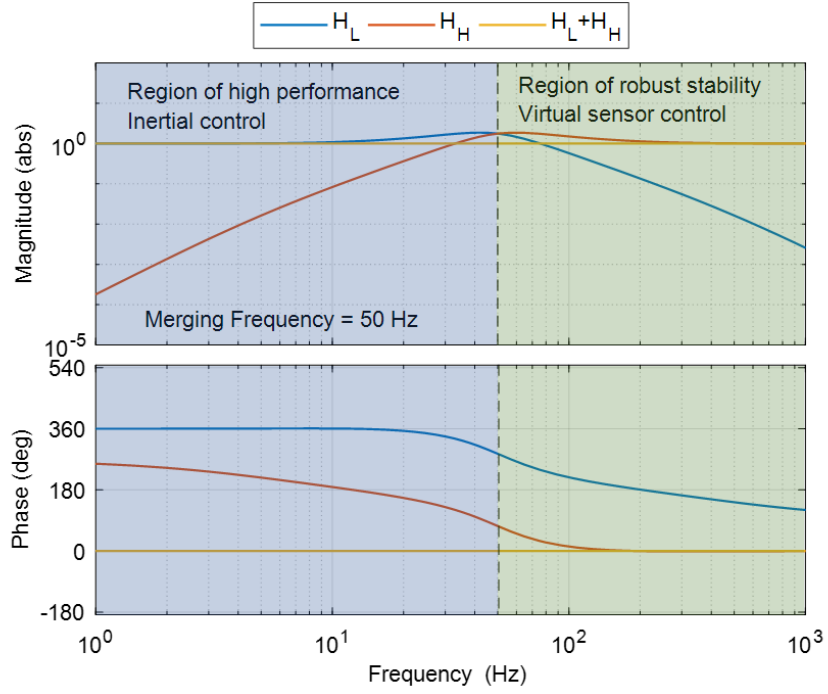


Figure 3: Frequency response of complementary filters. The blue colored region is dominated by inertial control and the green colored region by virtual sensor control. The merging frequency is at 50 Hz.

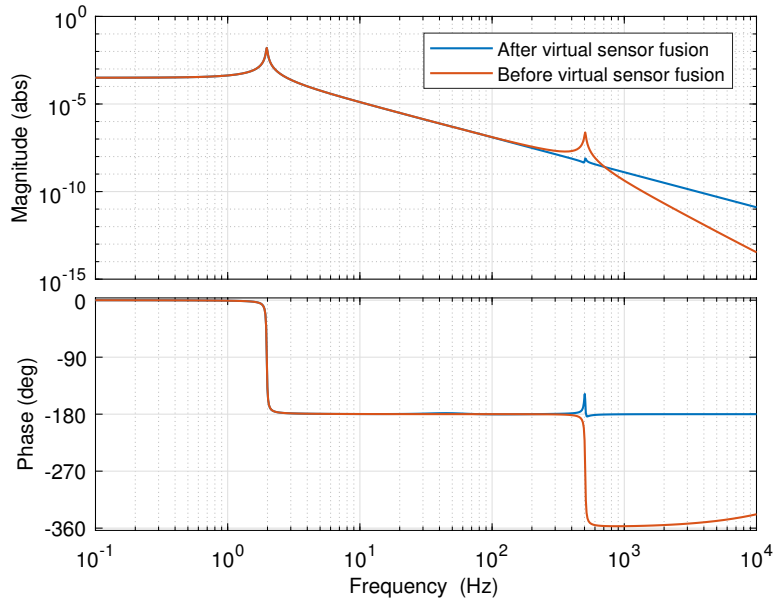


Figure 4: Frequency response of the plant before fusion ( $G_u$ ) and the plant after fusion ( $G_v H_H + G_u H_L$ ). It can be seen that there is no degradation of phase beyond  $-180^\circ$  in case of virtual sensor fusion.

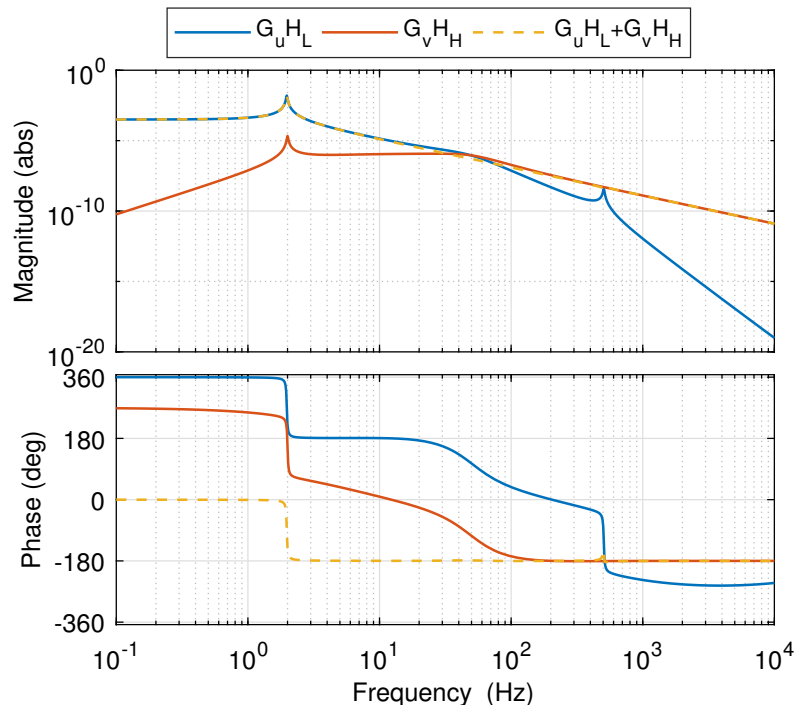


Figure 5: Comparison of the transfer function  $G_u H_L$ ,  $G_v H_H$  and  $G_u H_L + G_v H_H$ . The comparison shows the contributions from the real and virtual sensor control in the overall control input to the system.

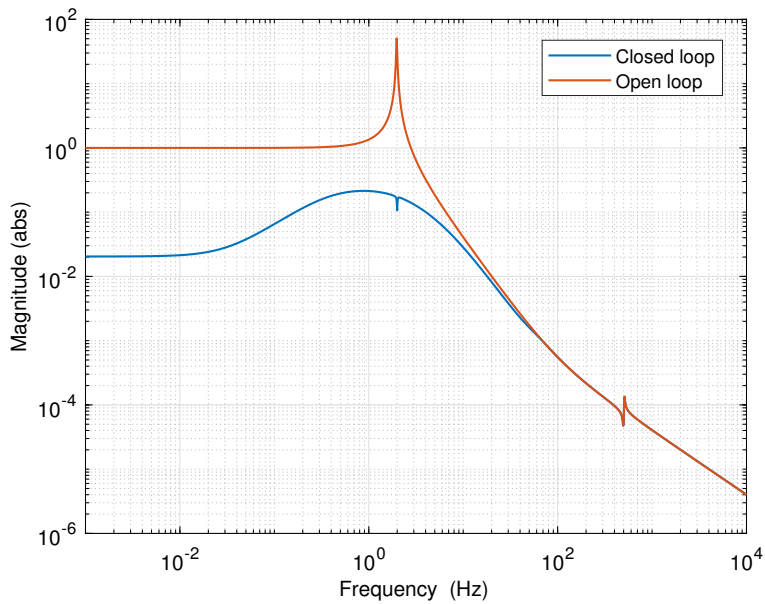


Figure 6: Comparison of transmissibility for the open and closed loop system. Note that virtual sensor fusion is able to reduce the transmissibility by a factor of nearly 100 at low frequency.

tion of the virtual plant ( $G_v$ ). In other words, the high frequency peak of  $G_u$  can be seen as spurious resonance introduced in the system due to sensor dynamics. This is treated as the unmodeled dynamics. To account for unmodeled dynamics (for example, phase lag and high frequency resonances), the plant ( $G_u$ ) can be represented mathematically using multiplicative uncertainty model [23] given by

$$\tilde{G}_u = G_v(1 + \Delta(s)W(s)) \quad (15)$$

where,  $\tilde{G}_u$  is a set of perturbed models of the plant;  $\Delta$  is a variable and stable transfer function satisfying  $\|\Delta\|_\infty \leq 1$ ; and  $W$  is a stable weighting transfer function.

The weighting function,  $W$ , is selected such that it covers all the unmodeled dynamics of the plant. The modeling errors are usually negligible at low frequency. These errors tend to increase with the frequency. Therefore, the obvious choice of the weighting function is a high pass filter. In the present case, the real plant has a spurious resonance at about 500 Hz with the peak magnitude less than 35 dB. The cutoff frequency of the weighting functions is set to 400 Hz. The magnitude of the weighting transfer function is adjusted to cover all the unmodeled dynamics. The weighting transfer function,  $W(s)$ , is

$$W(s) = \frac{70s^2}{(s + 2\pi \cdot 400)^2} \quad (16)$$

The magnitude of the frequency response of real, nominal and perturbed plants are compared in Figure 7. It can be seen that the perturbed plants cover the spurious resonance of the real plant. The nominal loop gain ( $L_n$ ) of the plant can be obtained by substituting  $G_u = G_v$  in  $L$ . That is,

$$\begin{aligned} L_n &= K(G_v H_L + G_v H_H) \\ &= K G_v (H_L + H_H) \\ &= K G_v \end{aligned} \quad (17)$$

The loop gain of the perturbed models of the plant ( $L_p$ ) can be written as

$$\begin{aligned} L_p &= K(\tilde{G}_u H_L + G_v H_H) \\ &= K(G_v(1 + \Delta(s)W(s))H_L + G_v H_H) \\ &= K(G_v H_L + G_v H_H + G_v \Delta(s)W(s)H_L) \\ &= L_n + K G_v \Delta(s)W(s)H_L \end{aligned} \quad (18)$$

The graphical representation of the robust stability analysis is shown in Figure 8. The blue line corresponds to the Nyquist plot of the nominal loop gain ( $L_n$ ). The red circle with the unity radius

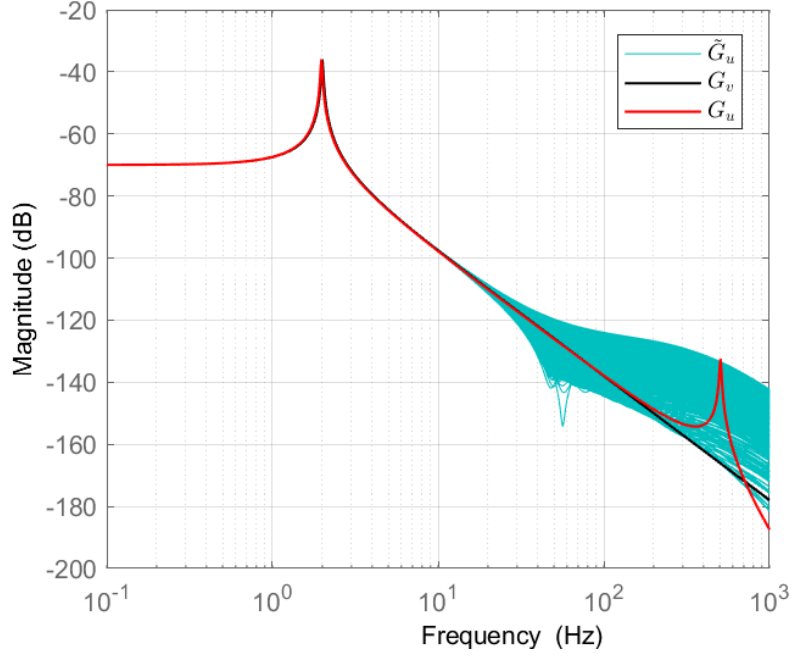


Figure 7: Bode magnitude plot of nominal plant ( $G_v$ ), real plant ( $G_u$ ) with spurious resonance and the perturbed plants ( $\tilde{G}_u$ ). Notice that perturbed plants covers the unmodeled dynamics of the real plant.

defines the stability limit. The black dotted circles represent the uncertainty disk at each frequency, whose radius is equal to [24]

$$U_r = |KG_v W(s)H_L| \quad (19)$$

Note that the uncertainties are incorporated only at low frequency. This is due to the fact that the signals from the real plant are only used at low frequency. Virtual sensor is used at high frequency. The stability margin is defined as the minimum angle at which uncertainty disk intersects the unit radius circle centered at origin on the Nyquist plot. It can be seen that even in the presence of uncertainties, the stability margins of the system are not much affected in virtual sensor fusion. To summarize, the algorithm for virtual sensor fusion is given in Algorithm 1.

## 5. Experimental validation

This section presents an experimental implementation of the virtual sensor fusion technique. The aim of the experiment is to actively isolate a pendulum from the ground motion.

---

**Algorithm 1:** Algorithm for virtual sensor fusion

---

**Input:** Nominal plant transfer function  $G_u$

- 1 Select the transfer function for the virtual sensor,  $G_v$ , based on the response desired at high frequency (can also be taken as nominal model of the plant)
- 2 Select the degree of the complementary high and low pass filters ( $H_H, H_L$ ). Usual choice is 2- or 3-order filter. Select the blending frequency below which we have a good model of the plant
- 3 Design the complementary filters
- 4 Design a lead-lag compensator for the plant ensuring high gain at low frequencies and sufficient margins at high frequencies.
- 5 Plot the loop gain for virtual sensor fusion and check if sufficient gain and phase margins are achieved.
- 6 Construct the weighting transfer function ( $W$ ) such that the perturbed plant,  $\tilde{G}_u = G_v(1 + \Delta(s)W(s))$ , covers the unmodeled dynamics of the real plant.
- 7 Plot the Nyquist diagram of the loop gain with the uncertainty disk having radius  $|KG_vWH_L|$  for all frequencies. Check if the critical point  $(-1, 0j)$  lies outside the disk of uncertainties. Also, check if the minimum phase margin is assured. Minimum phase margin can be obtained as the minimum angle at which the uncertainty disk intersect the unity gain circle.
- 8 If the robust stability margins in *Step 6* are not achieved, reduce the blending frequency and repeat *Steps 2 to 6*.

---

Note that higher order filters results in higher amplitude of the filters near the blending frequency. This may affect the closed loop performance of the system near the merging frequency. The order of the filter needs to be high enough such that the control is fully dominated by the sensor of interest and low enough to ensue good closed loop performance.

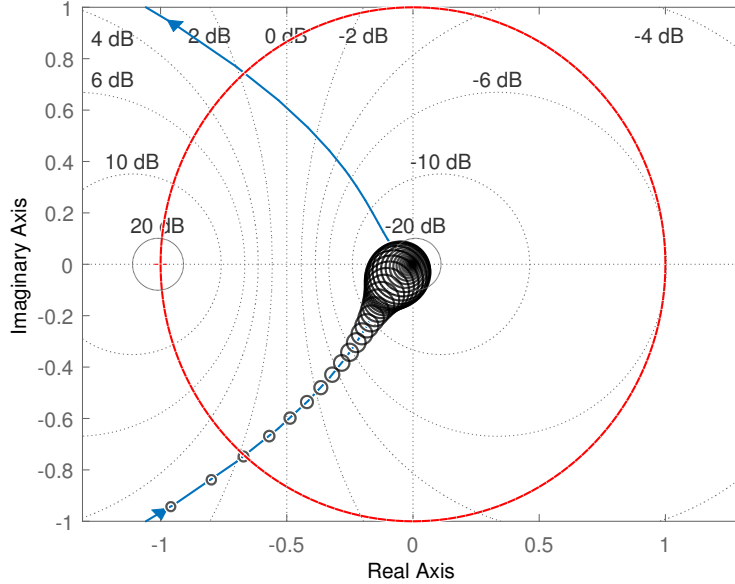


Figure 8: Graphical representation of the robust stability analysis for virtual sensor fusion — it can be seen that even in the presence of the uncertainties, the stability margins of the system are not much affected in virtual sensor fusion.

### 5.1. Test setup

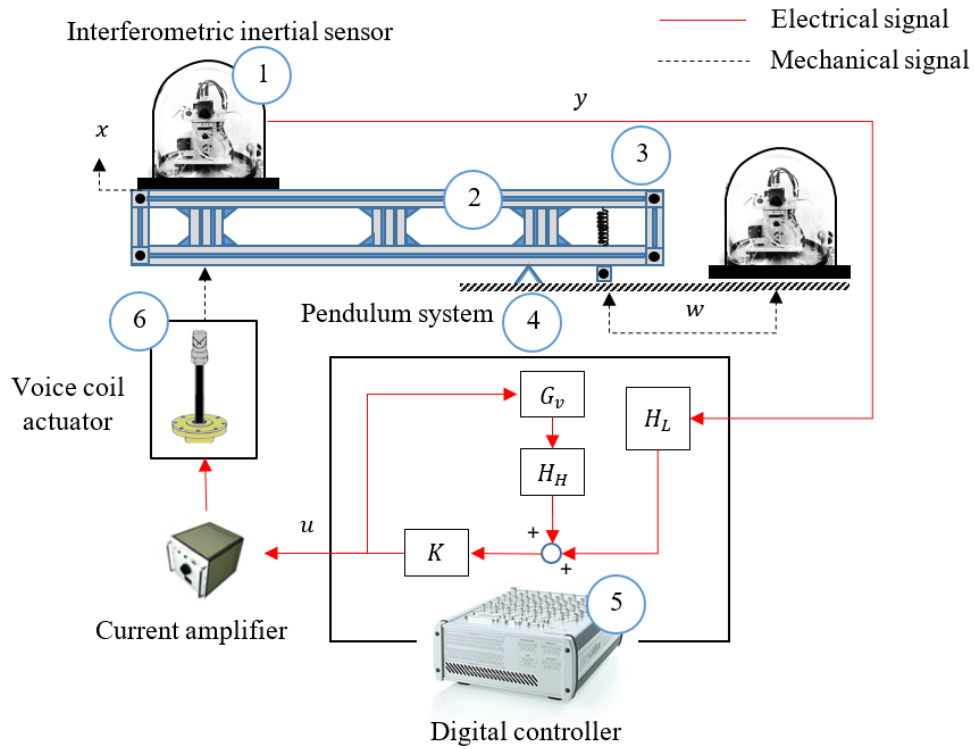
The experiment using virtual sensor fusion was carried out on a pendulum system shown in Figure 9. It represents a simple lever system with beam acting as a lever and a wedge as fulcrum. The masses of the beam and inertial sensor are supported by a spring. The motion of the host structure (i.e, the tip of the beam, on the other side of the spring) was isolated from the ground motion using virtual sensor fusion. A voice coil actuator was used to control the host structure motion. A customized high-resolution interferometric inertial sensor [25, 26], developed in-house, was used for measuring inertial motion of the host structure. The inertial ground motion was also measured using a similar sensor. The sensor on the pendulum had two sensing units - loop sensor used for feedback and monitor sensor used for monitoring purpose. The interferometer provided two quadrature signals. The inertial motion is related to the phases of those quadrature signals. The resolution of the interferometric sensor used was  $10^{-12}m/\sqrt{Hz}$  at 1 Hz. The controller was implemented in real-time using dSpace MicroLabBox, which was also used for data acquisition. The signals were measured with a sampling frequency of 1 kHz.

## 5.2. Control strategy

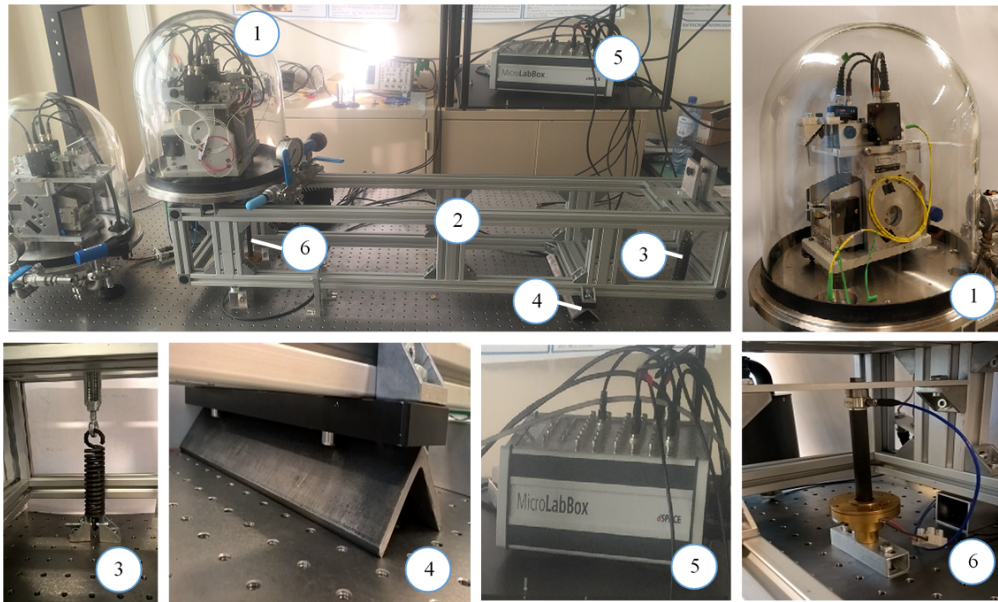
The main objective of the experiment was to have good isolation performance at low frequency while ensuring the robustness of the system to spurious resonances at high frequency. A good knowledge of the plant is available up to 7 Hz. First order complementary filters were used for virtual sensor fusion (higher order filters were not realized at the time of the experiments). It was found that the attenuation due to the first order filter was not significant. In order to use first order filter, one needs to have good knowledge of the plant near the merging frequency to realize the desired level of attenuation. Therefore, the merging frequency for the complementary filters was selected as 5 Hz. The knowledge of the plant near the merging frequency was injected in the controller using notch filters. The low pass filter was augmented with a lag compensator and notch filter while the high pass filter was augmented with a lead compensator and a notch filter near to merging frequency. It should be noted that the modification of the low and high pass filters will not be necessary if higher order complementary filters are used. The transfer functions from inertial control times low pass filter, virtual sensor control times high pass filter and virtual sensor fusion (i.e, the sum of low frequency inertial control and high frequency virtual sensor control) to the host structure motion are compared in Figure 10. A lot of fluctuations are observed in the magnitude and phase response of the inertial control ( $G_u H_L$ ) above 20 Hz which can affect the stability of the system at high frequency. On the other hand, the virtual sensor fusion control ( $G_u H_L + G_v H_H$ ) is found to be smooth and devoid of any such fluctuations at high frequency. Thus, ensuring the robustness of the system at high frequency.

## 5.3. Results

The amplitude spectral densities (ASDs) of the host structure as recorded by the interferometric sensor with and without control are shown in Figure 11. It is observed that the ASD measured with the loop sensor is lower than that measured with the monitor sensor. The noise of the loop sensor drives the actuator which in turn forces the host structure to follow the noise. Monitor sensor provides a better representation of the inertial motion of the host structure. The virtual sensor fusion is able to attenuate the motion of the host structure by ten times around 0.1 Hz. This demonstrates the effectiveness of the proposed strategy. The transmissibilities between the host structure and ground motions with and without control are compared in Figure 12. A good isolation performance is observed for the frequencies less than 3 Hz.



(a)



(b)

Figure 9: Experimental setup— (a) schematic diagram and (b) actual setup. The setup consists of a SDOF pendulum system. Interferometric sensors are used to sense the motion of the ground and the tip of the pendulum. The controller designed using virtual sensor fusion is implemented using real-time target machine. Voice coil actuator is used to control the motion of the host structure.

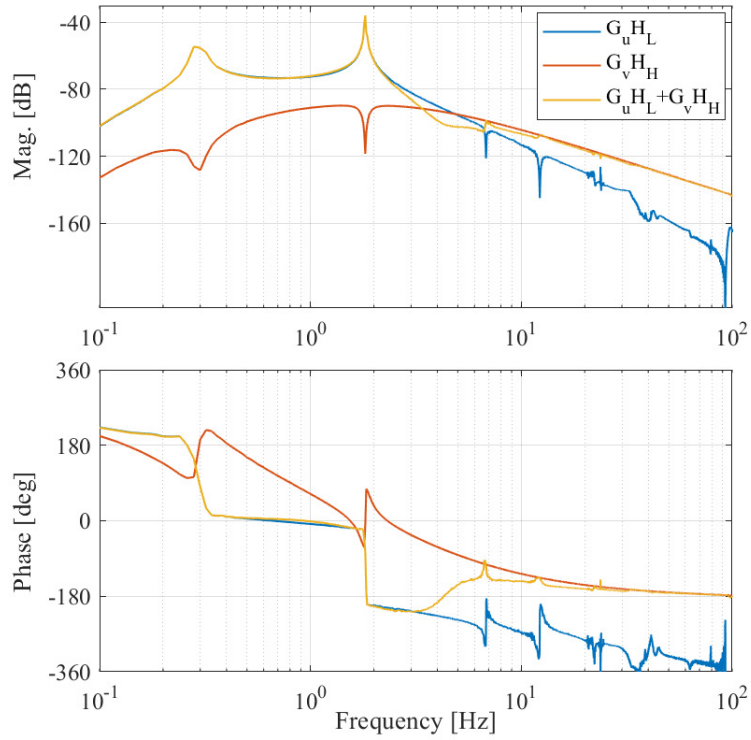


Figure 10: Comparison of the transfer functions from inertial control, virtual sensor control and their fusion to host structure motion

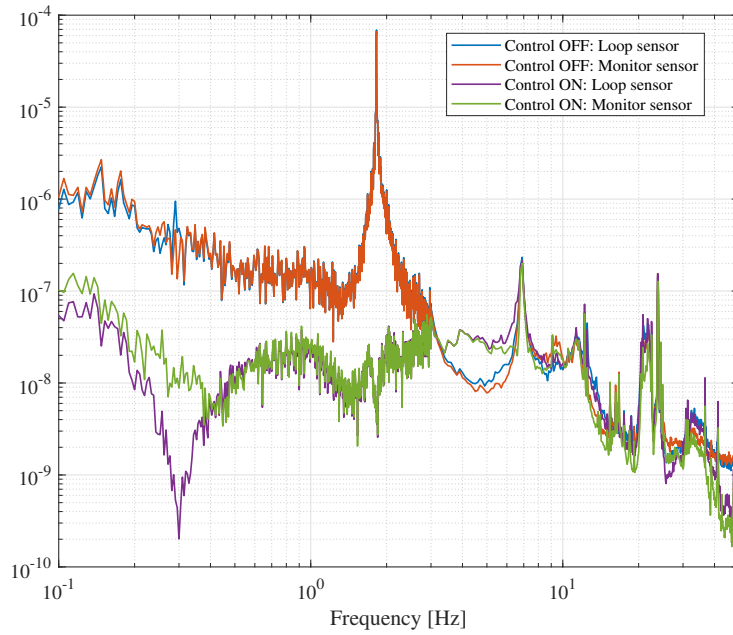


Figure 11: ASD of the host structure motion measured using interferometric inertial sensor with and without active control

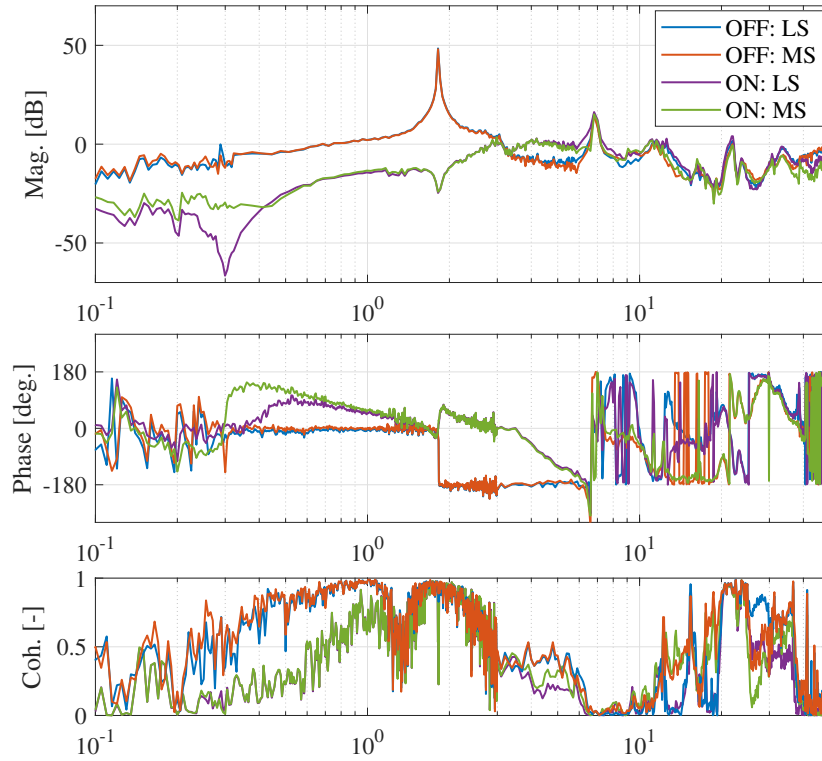


Figure 12: Comparison of the transfer function from ground motion to the host structure motion with and without active control (MS: Monitor sensor, LS: Loop sensor)

## 6. Concluding remarks

A new technique, termed as “virtual sensor fusion”, has been presented in which the signal from real and virtual sensors are fused in synergy to achieve good performance at lower frequencies while ensuring the stability of the system at high frequencies. The real sensor is chosen as inertial sensor while the virtual is simply a stable transfer function exhibiting desired high frequency response. The real and virtual sensors are augmented with high and low pass complementary filters such that the control at low frequency is dominated by the inertial sensor and at high frequency by the virtual sensor. The merging frequency of the two filters is usually taken as the frequency below which the dynamics of the real plant are well represented by its model. Since the control action at high frequency is dominated by the virtual sensor, the effect of spurious resonances that might exist at high frequency (unmodeled dynamics) does not appear in the feedback loop. Hence, the stability and robustness of the system is ensured in the high frequency region. The effectiveness of the proposed control strategy is demonstrated by applying it to the active seismic vibration

isolation system. A robustness analysis is also carried out by representing unmodeled dynamics as multiplicative uncertainties and evaluating guaranteed stability margins. Finally, the experimental validation of virtual sensor fusion is carried out on a pendulum system. Virtual sensor fusion is found to reduce the transmissibility by an order of 10 at lower frequencies while keeping the system robustly stable. The future work will focus on the design of higher order complementary filters through optimization to achieve desired trade-off between performance and robustness. This technique can be further generalized to multi-input multi-output (MIMO) systems.

## **Acknowledgements**

The authors gratefully acknowledge the French Community for financing FRIA grant of Jennifer Watchi (grant number FC 27289) and Thomas Dehaeze (grant number FC 31597). Authors also acknowledge FRS-FNRS for funding this research (grant agreement F.4536.17). The authors would like also to thank the Klaus Stammler and Edgar Wetzig from the Federal Institute for Geosciences and Natural Resources in Hannover and Michel Can Camp from the Royal Observatory of Belgium for lending STS-1V seismometers for the tests.

## **Reference**

- [1] X. Li, Simultaneous, fault-tolerant vibration isolation and pointing control of flexure jointed hexapods, Ph.D. thesis, University of Wyoming (2000).
- [2] C. Collette, K. Artoos, A. Kuzmin, S. Janssens, M. Sylte, M. Guinchard, C. Hauviller, Active quadrupole stabilization for future linear particle colliders, *Nuclear Instruments and Methods in Physics Research Section A: Accelerators, Spectrometers, Detectors and Associated Equipment* 621 (1-3) (2010) 71–78.
- [3] F. Matichard, B. Lantz, K. Mason, R. Mittleman, B. Abbott, S. Abbott, E. Allwine, S. Barnum, J. Birch, S. Biscans, et al., Advanced ligo two-stage twelve-axis vibration isolation and positioning platform. part 2: Experimental investigation and tests results, *Precision engineering* 40 (2015) 287–297.
- [4] L. Vaillon, C. Philippe, Passive and active microvibration control for very high pointing accuracy space systems, *Smart materials and structures* 8 (6) (1999) 719.

- [5] W. B. Gevarter, Basic relations for control of flexible vehicles, *AIAA journal* 8 (4) (1970) 666–672.
- [6] F. Matichard, B. Lantz, K. Mason, R. Mittleman, B. Abbott, S. Abbott, E. Allwine, S. Barnum, J. Birch, S. Biscans, D. Clark, D. Coyne, D. DeBra, R. DeRosa, S. Foley, P. Fritschel, J. Giaime, C. Gray, G. Grabeel, J. Hanson, M. Hillard, J. Kissel, C. Kucharczyk, A. Le Roux, V. Lhuillier, S. Macinnis, B. O'Reilly, D. Ottaway, H. Paris, M. Puma, H. Radkins, C. Ramet, M. Robinson, L. Ruet, P. Sareen, D. Shoemaker, A. Stein, J. Thomas, M. Vargas, J. Warner, Design and performance overview of advanced ligo two-stage vibration isolation and alignment system, ASPE Conference.
- [7] J. F. Yocum, L. I. . Slafer, Control system design in the presence of severe structural dynamics interactions, *Journal of Guidance, Control, and Dynamics* 1 (2) (1978) 109–116.
- [8] L. Zuo, Element and system design for active and passive vibration isolation, Ph.D. thesis, Massachusetts Institute of Technology (2004).
- [9] N. Robertson, P. Fritschel, B. Shapiro, C. Torrie, M. Evans, Design of a tuned mass damper for high quality factor suspension modes in advanced ligo, *Review of Scientific Instruments* 88 (3) (2017) 035117.
- [10] H. Frahm, Improved means for damping the vibrations of bodies, Patent No. GB190923828.
- [11] W. Hua, Low frequency vibration isolation and alignment system for advanced ligo, Ph.D. thesis, stanford University (2005).
- [12] D. Tjepkema, J. van Dijk, H. Soemers, Sensor fusion for active vibration isolation in precision equipment, *Journal of Sound and Vibration* 331 (4) (2012) 735–749.
- [13] G. Losurdo, G. Calamai, E. Cuoco, L. Fabbroni, G. Guidi, M. Mazzoni, R. Stanga, F. Vetrano, L. Holloway, D. Passuello, et al., Inertial control of the mirror suspensions of the virgo interferometer for gravitational wave detection, *Review of Scientific Instruments* 72 (9) (2001) 3653–3661.
- [14] C. Collette, F. Matichard, Sensor fusion methods for high performance active vibration isolation systems, *Journal of sound and vibration* 342 (2015) 1–21.

- [15] Y.-S. Lee, S. Elliott, Active position control of a flexible smart beam using internal model control, *Journal of Sound and Vibration* 242 (5) (2001) 767–791.
- [16] R. De Keyser, C. Copot, A. Hernandez, C. Ionescu, Discrete-time internal model control with disturbance and vibration rejection, *Journal of Vibration and Control* 23 (1) (2017) 3–15.
- [17] T. H. Lee, T. S. Low, A. Al-Mamun, C. Tan, Internal model control (imc) approach for designing disk drive servo-controller, *IEEE Transactions on Industrial Electronics* 42 (3) (1995) 248–256.
- [18] S. Endo, H. Kobayashi, C. Kempf, S. Kobayashi, M. Tomizuka, Y. Hori, Robust digital tracking controller design for high-speed positioning systems, *Control Engineering Practice* 4 (4) (1996) 527–536.
- [19] J. Back, H. Shim, Adding robustness to nominal output-feedback controllers for uncertain nonlinear systems: A nonlinear version of disturbance observer, *Automatica* 44 (10) (2008) 2528–2537.
- [20] C. Bohn, A. Cortabarría, V. Härtel, K. Kowalczyk, Active control of engine-induced vibrations in automotive vehicles using disturbance observer gain scheduling, *Control Engineering Practice* 12 (8) (2004) 1029–1039.
- [21] B. A. Guvenc, L. Guvenc, Robust two degree-of-freedom add-on controller design for automatic steering, *IEEE Transactions on Control Systems Technology* 10 (1) (2002) 137–148.
- [22] M. T. White, M. Tomizuka, C. Smith, Improved track following in magnetic disk drives using a disturbance observer, *IEEE/ASME Transactions on mechatronics* 5 (1) (2000) 3–11.
- [23] J. R. Ryoo, T.-Y. Doh, M. J. Chung, Robust disturbance observer for the track-following control system of an optical disk drive, *Control Engineering Practice* 12 (5) (2004) 577–585.
- [24] J. C. Doyle, B. A. Francis, A. R. Tannenbaum, *Feedback control theory*, Courier Corporation, 2013.

- [25] B. Ding, G. Zhao, Zhao, J. Watchi, C. Collette, Huddle test of optical inertial sensors combined with slightly damped mechanics, Proceedings of ISMA2018 and USD2018 (2018) 1471–1478.
- [26] B. Ding, J. Watchi, C. Collette, Development of a high resolution optical inertial sensor, in: Proceedings of 7th World Conference on Structural Control and Monitoring, 7WCSCM, Qingdao, China, 2018, p. Paper No. 263.